ELSEVIER

NeuroImage

www.elsevier.com/locate/ynimg
NeuroImage 25 (2005) 1310–1324

Modeling both the magnitude and phase of complex-valued fMRI data

Daniel B. Rowe

Department of Biophysics, Medical College of Wisconsin, 8701 Watertown Plank Road, Milwaukee WI 53226-0509, USA

Received 19 November 2004; revised 27 December 2004; accepted 7 January 2005
Available online 19 March 2005

In MRI and fMRI, images or voxel measurement are complex valued or bivariate at each time point. Recently, (Rowe, D.B., Logan, B.R., 2004. A complex way to compute fMRI activation. NeuroImage 23 (3), 1078–1092) introduced an fMRI magnitude activation model that utilized both the real and imaginary data in each voxel. This model, following traditional beliefs, specified that the phase time course were fixed unknown quantities which may be estimated voxel-by-voxel. Subsequently, (Rowe, D.B., Logan, B.R., 2005. Complex fMRI analysis with unrestricted phase is equivalent to a magnitude-only model. NeuroImage 24 (2), 603–606) generalized the model to have no restrictions on the phase time course. They showed that this unrestricted phase model was mathematically equivalent to the usual magnitude-only data model including regression coefficients and voxel activation statistic but philosophically different due to it derivation from complex data. Recent findings by (Hoogenrad, F.G., Reichenbach, J.R., Haacke, E.M., Lai, S., Kuppusamy, K., Sprenger, M., 1998. In vivo measurement of changes in venous blood-oxygenation with high resolution functional MRI at .95 Tesla by measuring changes in susceptibility and velocity. Magn. Reson. Med. 39 (1), 97–107) and (Menon, R.S., 2002. Postacquisition suppression of large-vessel BOLD signals in high-resolution fMRI. Magn. Reson. Med. 47 (1), 1–9) indicate that the voxel phase time course may exhibit task related changes. In this paper, a general complex fMRI activation model is introduced that describes both the magnitude and phase in complex data which can be used to specifically characterize task related change in both. Hypotheses regarding task related magnitude and/or phase changes are evaluated using derived activation statistics. It was found that the Rowe–Logan complex constant phase model strongly biases against voxels with task related phase changes and that the current very general complex linear phase model can be cast to address several different hypotheses sensitive to different magnitude/phase changes.

Keywords: Complex-valued fMRI data; Rowe–Logan complex; Magnitude changes; Phase changes

Introduction

It is well known that in magnetic resonance imaging (MRI) and functional magnetic resonance imaging (fMRI), images or voxel measurements are complex valued or bivariate due to phase imperfections and thus in fMRI, voxel time course measurements appear in both the real and imaginary channels (Bernstein et al., 1989; Haacke et al., 1999; Macovski, 1996). An example of a voxel's complex valued time course with assumed magnitude task related changes and a constant phase is presented in Fig. 1, where the length of the vector from the origin to the point in real-imaginary space is the magnitude and the angle the vector makes with the real axis is the phase. In fMRI, the real and imaginary components are the quantities that are measured with observation error. For example in a block design finger tapping experiment, the vector described by the arrow in Fig. 1 appears to "jitter" around in a lower vector length state during the control task than the length of this vector appears to "jitter" around in a higher vector length state. Any apparent "jitter" in the phase would be purely from measurement error in the real and imaginary components of the vector. In fMRI, complex valued voxel time courses are generally converted to magnitude and phase time courses then task related magnitude-only data activation determined with the phase voxel time course discarded (Bandettini et al., 1993; Cox et al., 1995). The original complex data are unrecoverable after discarding the phase and the magnitude-only operation is nonunique. Other attempts have been made to avoid complex voxel time courses such as phasing them into the real channel (Bernstein et al., 1989).

Rowe and Logan (2004) introduced a general complex fMRI magnitude activation model in which multiple regressors were allowed using the standard general linear statistical model, hypothesis tests were formulated in terms of contrasts, and the phase was directly modeled as a fixed unknown quantity which may be estimated voxel by voxel (Rowe and Logan, 2004). Furthermore, a large sample Chi-square distributed statistic was presented for comparability between the two models. In Rowe and Logan (2005), the complex model was generalized to have an unrestricted phase time course (Rowe and Logan, 2005). They showed that this model was mathematically equivalent to the usual magnitude-only data model in terms of regression coefficients and

E-mail address: dbrowe@mcw.edu.
Available online on ScienceDirect (www.sciencedirect.com).

1053-8119/$ - see front matter © 2005 Elsevier Inc. All rights reserved.
doi:10.1016/j.neuroimage.2005.01.034

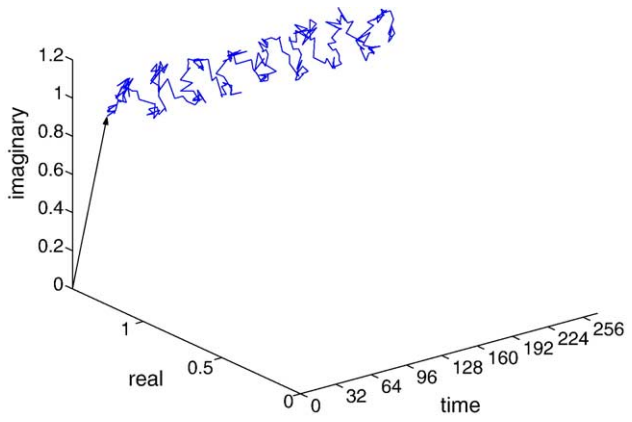

Fig. 1. Complex valued voxel time course.

voxel activation statistic but philosophically different due to its derivation from complex data. The magnitude-only or equivalently complex unrestricted phase data models only utilize information in the magnitude through the exact Ricean distribution or through the large signal-to-noise ratio (SNR) normal distribution approximation (Gudbjartsson and Patz, 1995; Rice, 1944). Parameter estimation in the complex constant phase model and the magnitude-only or equivalently complex unrestricted phase data model were examined in Rowe (2005). Rowe (2005) found that the magnitude-only data model with a normal approximation to a Ricean distribution exhibited decreased activation detection power at lower SNRs when compared to the complex constant phase model but a Taylor series approximation to the Ricean distribution showed modest improvement (Rowe, 2005).

However, Hoogenrad et al. (1998) and Menon (2002) presented evidence to suggest that the voxel phase angle time courses may not be exactly constant over time but may also exhibit task related phase changes in voxels with "large" vessels (Hoogenrad et al., 1998; Menon, 2002). This is the motivation for this work. Specifically, a model is developed to help us characterize voxels in terms of task related magnitude and/or phase changes. Voxels in parenchyma with task related magnitude changes are of primary interest, but voxels with task related phase changes, although not of interest in themselves, their characterization helps us identify voxels that only have task related magnitude changes that are of interest.

In this paper, a general complex fMRI activation model is introduced that describes both the magnitude and phase which can be used to specifically model and test for task related changes in the magnitude, the phase, or both the magnitude and phase. Thus, in principle, activation can be determined from voxels with "small" vessels such as those in the capillary bed of parenchymal tissue having solely magnitude changes and not voxels with "large" vessels having task related changes in both the magnitude and phase. This implies that the phase may contain information about the brain that is not present in the magnitude of the response. The situation of the vector valued voxel observation residing in the two magnitude length states is depicted in Fig. 2a while the situation of the two vector states that involve a lengthening and rotation is depicted in Fig. 2b. Where for example, the magnitude and phase are described by linear models with x_t' being the t^{th} row of a design matrix $\mathbf{X}$ having, for example, a column of ones, a column of counting numbers, and a square wave reference function with corresponding coefficients (β_0, β_1, β_2) and (γ_0, γ_1, γ_2). The activation model from magnitude-only data is sensitive to voxels that have task related changes in the magnitude regardless of whether there are changes of any kind in the phase, while magnitude activation from complex data specifically describes and dictates whether or not we wish to include voxels that have task related phase changes. Menon sought to account for changes in the observed magnitude that could be accounted for by changes in the phase by including voxel phase values as a random independent regressor variable in a least squares model (Menon, 2002).

In fMRI, we seek voxels with small vessels in parenchymal tissue having random orientations whose phase contributions are small in aggregate. Thus, in principle, the phase angle

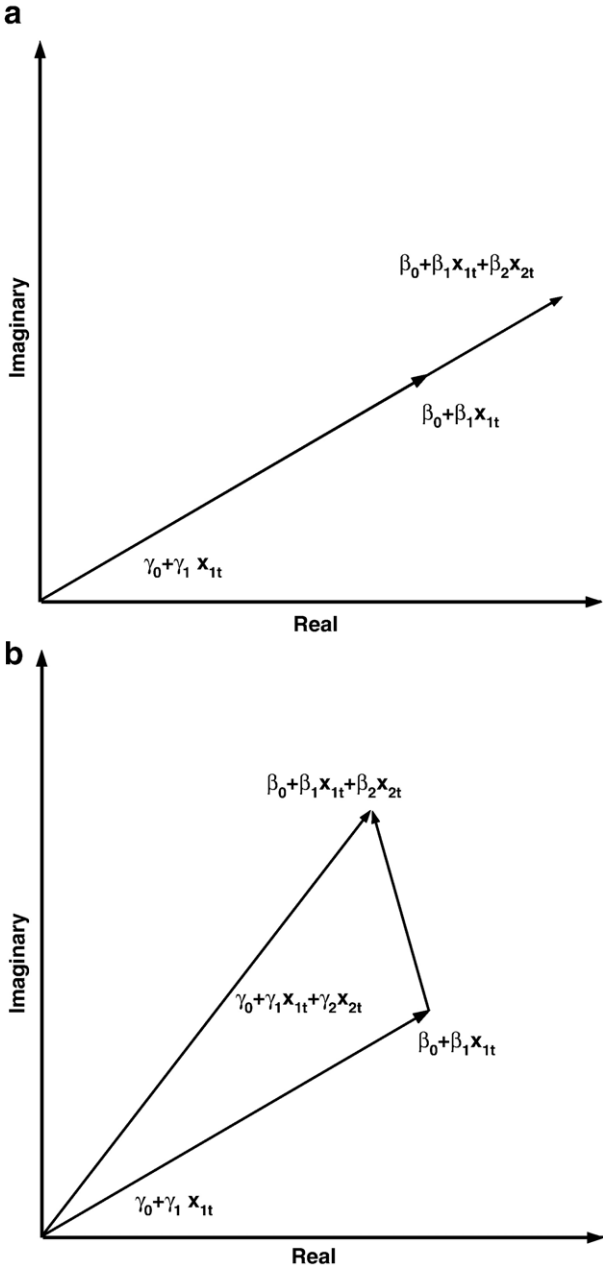

Fig. 2. Task related magnitude/phase changes. (a) Magnitude-alone change. (b) Magnitude and phase change.

contains information about the vasculature in the vicinity of the voxel. It is this information that is sought to be modeled and utilized. A generalization of the Rowe–Logan complex activation models (Rowe and Logan, 2004, 2005) is developed where the phase angle can be described with a linear model where task related changes in the phase can be quantified. With this model, several pairs of hypotheses can be tested including determining voxels that exhibit task related magnitude-alone changes, phase-alone changes, along with task related magnitude and/or phase changes. Task related magnitude and/or phase activation maps can be generated from complex valued voxel time courses and an appropriate threshold determined (Logan and Rowe, 2004).

Results of the proposed complex linear phase model with five different hypothesis pairs are compared to a complex unrestricted phase or strict magnitude-only data model, a phase-only data model, and the Rowe–Logan complex constant phase data model in terms of (1) thresholded activation maps for a real dataset then (2) activation power for simulated data. The simulations are performed with several magnitude contrast-to-noise ratios (CNRs) and task related phase changes (TRPC) for two different signal-to-noise ratios (SNRs).

Model

As previously noted, in MRI/fMRI due to random noise, phase imperfections, and possible biophysical processes that produce phase signal variation, we obtain a complex valued measured object that consists of a true complex valued object plus complex valued noise.

Neglecting the voxel location and focusing on an individual voxel, the complex valued image $\boldsymbol{y}_t$ measured over time t can be described with a nonlinear multiple regression model that includes both a temporally varying magnitude ρ_t and phase θ_t given by

$$y_t = [\rho_t \cos\theta_t + \boldsymbol{\eta}_{Rt}] + i[\rho_t \sin\theta_t + \boldsymbol{\eta}_{It}]$$

$$\rho_t = x_t' \boldsymbol{\beta} = \boldsymbol{\beta}_0 + \boldsymbol{\beta}_1 x_{1t} + \cdots + \boldsymbol{\beta}_{q1} x_{q_1 t}$$

$$\theta_t = u_t' \boldsymbol{\gamma} = \boldsymbol{\gamma}_0 + \boldsymbol{\gamma}_1 u_{1t} + \cdots + \boldsymbol{\gamma}_{q2} u_{q_2 t}, \qquad t = 1,\ldots,n \tag{2.1}$$

where $(\boldsymbol{\eta}_{Rt}, \boldsymbol{\eta}_{It})' \sim \mathcal{N}(0, \Sigma)$, x_t' is the t^{th} row of an $n \times (q_1 + 1)$ design matrix $\mathbf{X}$ for the magnitude, u_t' is the t^{th} row of an $n \times (q_2 + 1)$ design matrix $\mathbf{U}$ for the phase, and $\sum = \sigma^2 I_2$ while $\boldsymbol{\beta}$ and $\boldsymbol{\gamma}$ are magnitude and phase regression coefficient vectors respectively. Note that a separate design matrix $\mathbf{U}$ for the phase has been incorporated but $\mathbf{X}$ and $\mathbf{U}$ can be the same. If $\boldsymbol{\gamma}_j = 0$ for $j = 1,\ldots, q_2$ then this becomes the Rowe–Logan constant phase model. The complex valued observation $\boldsymbol{y}_t$ can be represented at time point t as a 2×1 vector instead of as a complex number

$$\begin{pmatrix} y_{Rt} \\ y_{It} \end{pmatrix} = \begin{pmatrix} \rho_t \cos\theta_t \\ \rho_t \sin\theta_t \end{pmatrix} + \begin{pmatrix} \boldsymbol{\eta}_{Rt} \\ \boldsymbol{\eta}_{It} \end{pmatrix}, \qquad t = 1,\ldots,n.$$

The distributional specification is on the real and imaginary parts of the voxel signal and not on the magnitude or length of a vector. The phase signal in Eq. (2.1) is a temporally varying quantity, which is described with a general linear model and estimated voxel by voxel.

The Rowe–Logan complex fMRI activation models can be written more generally as

$$\underset{2n\times 1}{y} = \underset{2n\times 2n}{\begin{pmatrix} \mathbf{A}_1 & 0 \\ 0 & \mathbf{A}_2 \end{pmatrix}} \underset{2n\times 2(q_1+1)}{\begin{pmatrix} \mathbf{X} & 0 \\ 0 & \mathbf{X} \end{pmatrix}} \underset{2(q_1+1)\times 1}{\begin{pmatrix} \boldsymbol{\beta} \\ \boldsymbol{\beta} \end{pmatrix}} + \underset{2n\times 1}{\boldsymbol{\eta}} \tag{2.2}$$

imaginary values and the vector of errors $\boldsymbol{\eta} = (\boldsymbol{\eta}_R', \boldsymbol{\eta}_I')' \sim \mathcal{N}(0, \Sigma \otimes \Phi)$ is similarly defined where $\otimes$ is the Kronecker product operation that multiplies every element of its first matrix argument by its entire second matrix argument. Here, we specify that $\Sigma = \sigma^2 I_2$ and $\Phi = I_n$. Furthermore, $\mathbf{A}_1$ and $\mathbf{A}_2$ are square diagonal matrices with t^{th} diagonal element $\cos\theta_t$ and $\sin\theta_t$ respectively.

Activation

Linearly constrained magnitude and/or phase hypotheses can be tested on an individual voxelwise basis with linear constraint matrices $\mathbf{C}$ for the magnitude coefficients and $\mathbf{D}$ for the phase coefficients that are of dimension $r_1 \times (q_1 + 1)$ and $r_2 \times (q_2 + 1)$ respectively. Model parameters are estimated under appropriately constrained null and alternative hypotheses then activation determined with a generalized likelihood ratio statistic. Denote the maximum likelihood estimators under the alternative hypothesis using hats and those under the null hypothesis using tildes. Then, the generalized likelihood ratio statistic as derived in Appendix A for this task related magnitude and/or phase complex fMRI activation model is

$$-2\log\lambda = 2n\log\left(\frac{\tilde{\boldsymbol{\sigma}}^2}{\hat{\boldsymbol{\sigma}}^2}\right). \tag{3.1}$$

This statistic has an asymptotic χ_r^2 distribution where r is the difference in the number of constraints between the alternative and null hypotheses. Denoting r_1 and r_2 as the full row ranks of $\mathbf{C}$ and $\mathbf{D}$ respectively, the degrees of freedom is either r_1, r_2, or $r_1 + r_2$.

With this model, there are four hypotheses that can readily be seen as presented in Table 1. The parameters are estimated under each of the hypotheses so that pairs of hypotheses can be used in a generalized likelihood ratio test. Hypothesis H_a places no constraints on either the magnitude or phase coefficients; hypothesis H_b places constraints on the magnitude coefficients but not on the phase coefficients; hypothesis H_c places constraints on the phase coefficients but not on the magnitude coefficients; hypothesis H_d places constraints on both the magnitude and phase coefficients. From the four hypotheses, five meaningful hypothesis pairs can be formed in which the parameter space of the null hypothesis is contained within the parameter space of the alternative hypothesis.

The hypothesis pair H_d vs. H_a should detect task related voxel activation either in the magnitude, the phase, or both since the parameters are estimated under the null hypothesis with magnitude and phase linear contrast equality constraints while under the alternative hypothesis without magnitude or phase linear contrast

Table 1
Some possible hypotheses for testing

H_a: $C\beta \neq 0$, $D\gamma \neq 0$
H_b: $C\beta = 0$, $D\gamma \neq 0$
H_c: $C\beta \neq 0$, $D\gamma = 0$
H_d: $C\beta = 0$, $D\gamma = 0$

equality constraints; H_d vs. H_b should detect task related voxel activation in the phase while focusing on voxels without task related magnitude changes since the parameters are to be estimated under both hypotheses with the magnitude linear contrast equality constraints; H_d vs. H_c should detect task related voxel activation in the magnitude while focusing on voxels without task related phase changes since the parameters are to be estimated under both hypotheses with the phase linear contrast equality constraints; H_c vs. H_a should detect task related voxel activation in the phase regardless of whether or not there is task related changes in the magnitude since the parameters are to be estimated under both hypotheses without any magnitude linear contrast equality constraints; H_b vs. H_a should detect task related voxel activation in the magnitude regardless of whether or not there is task related changes in the phase since the parameters are to be estimated under both hypotheses without any phase linear contrast equality constraints.

For example, consider a model with a magnitude design matrix with three columns, the first being ones, the second being counting numbers, and the last being a stimulus or task related reference function along with a phase design matrix that is identical to the magnitude one. The magnitude and phase regression coefficients β_0 and γ_0 represent intercepts; β_1 and γ_1 representing a linear drift over time; while β_2 and γ_2 represent task related effects. Then, for example, in hypothesis H_d, the linear coefficient constraints of H_d: $\beta_2 = 0$, $\gamma_2 = 0$ can be described by $\mathbf{C} = (0, 0, 1)$ and $\mathbf{D} = (0, 0, 1)$ so that the null hypothesis is H_d: $\beta_2 = 0$, $\gamma_2 = 0$. It should be noted that the Rowe–Logan (Rowe and Logan, 2004) complex constant phase model is equivalent to the hypothesis test of H_d vs. H_c with $\mathbf{D} = (0, I_{q_2})$ or H_b vs. H_a with $\mathbf{U} = (1,\ldots,1)'$ and $\mathbf{D} = 1$ while the complex unrestricted phase model is equivalent to a hypothesis test of H_b vs. H_a with $\mathbf{U} = I_n$ and $\mathbf{D} = I_n$.

The existing hypotheses of magnitude-only data activation and magnitude activation from complex data with constant phase are supported within this framework. This framework allows for additional hypotheses regarding task related activation in the magnitude and/or phase in complex data. As previously noted, voxels with task related magnitude and phase changes are potentially ones that contain large vessels and not those that we seek in parenchymal tissue with small vessels.

Real fMRI data

A bilateral sequential finger tapping experiment was performed in a block design with 16 s off followed by eight epochs of 16 s on and 16 s off. Scanning was performed using a 1.5T GE Signa in which 5 axial slices of size 96 × 96 were acquired with a full *k*-space single shot gradient echo pulse sequence having a FA = 90° and a TE = 47ms. In image reconstruction, the acquired data were zero filled to 128 × 128. After Fourier image reconstruction, each voxel has dimensions in of 1.5625 × 1.5625 × 5. Observations were taken every TR = 1000 ms so that there are 272 in each voxel. Data from a single axial slice through the sensorimotor cortex was selected for analysis. Preprocessing included the removal of the first three points to omit magnetic field equalization effects followed by the use of an ideal 0/1 frequency filter (Gonzales and Woods, 1992; Press et al., 1992) to remove respiration and low frequency physiological noise. Where necessary, the phase time courses were unwrapped for jumps greater than π between successive observations.

In Figs. 3a–c are 5% false discovery rate (FDR) thresholded χ^2-statistic maps with real fMRI data for (a) the complex unrestricted phase (UP) or usual magnitude-only data model; (b) a phase-only (PO) data model (activation from phase-only data assuming normality); (c) the Rowe–Logan complex constant phase (CP) activation model; along with overlap maps in (d)–(f) zoomed in to a central 64 × 64 section for (d) the models in (a) and (c); (e) the models in (a) and (b); and (f) the models in (b) and (c). Additionally, the same χ^2-statistic and overlap maps are presented in Figs. 4a–f except a 5% Bonferroni familywise error (FWE) rate thresholded is applied. In Figs. 3d–f and 4d–f, voxels that were above threshold only for the UP model are colored red, only for the CP model colored orange, only for the UP and CP models colored yellow, only for the PO model colored light blue, only for the UP and PO models colored pink, only for the CP and PO models colored dark blue.

In Figs. 3d and 4d, it can be seen that the voxels that are above threshold for the CP model are essentially a subset of those above threshold for the UP model. In Figs. 3e and 4e, it can be seen that the voxels that are above threshold for the UP model include many voxels that are also above threshold for the PO model. In Figs. 3f and 4f, it can be seen that the voxels that are above threshold for the CP model include very few voxels that are also above threshold for the PO model as compared to the UP model. These phenomena are more prominent for a Bonferroni FWE threshold. Summarizing, it can be seen from both the activation and overlap maps in Figs. 3 and 4 that the complex unrestricted phase model declares any voxels as active that have statistically significant TRPC and that the Rowe–Logan complex activation model with a constant phase biases against voxels with TRPC as seen by fewer voxels colored dark blue than pink.

For the same data, the χ^2 activation maps from the five hypothesis pairs from the current complex model (CM) are applied and presented in Figs. 5a–e. Different hypothesis pairs of the current complex linear TRPC model are sensitive to different things. The properties of this model are pictorially presented in Figs. 5 and 6. It can be seen that the hypothesis test pair H_d vs. H_c in Fig. 5c and the pair H_b vs. H_a in Fig. 5e are very similar to the CP activation map. This similarity is because, in the null hypotheses, there is no task related magnitude changes, and in the alternative hypotheses, there are unrestricted task related magnitude changes. Furthermore, the test pairs H_d vs. H_b in Fig. 5b and H_c vs. H_a in Fig. 5d are very similar to the PO activation map. This similarity is because, in the null hypotheses, there is no task related phase changes, and in the alternative hypotheses, there are unrestricted task related phase changes. In addition, the pair H_d vs. H_a in Fig. 5a appears to be a combined UP and PO activation map because the null hypotheses has no task related magnitude and/or phase changes and in the alternative hypotheses there are unrestricted task related magnitude and/or phase changes. In Fig. 5f is a two sided Bonferroni FWE corrected activation map for the PO model in which it can be noted that the activations in the sensorimotor area are positive (yellow) while others are negative (light blue) with a colorbar to the right. Perhaps one sided tests involving the phase are more appropriate.

In Figs. 6a–f are maps of overlapping voxels zoomed in for a central 64 × 64 portion that are above a 5% Bonferroni FWE threshold for the UP model, the PO model, and individually each of the maps given in Figs. 5a–e and 4a–c.

In Fig. 6, red indicates voxels that are above threshold only for the UP model; light blue indicates voxels that were above threshold

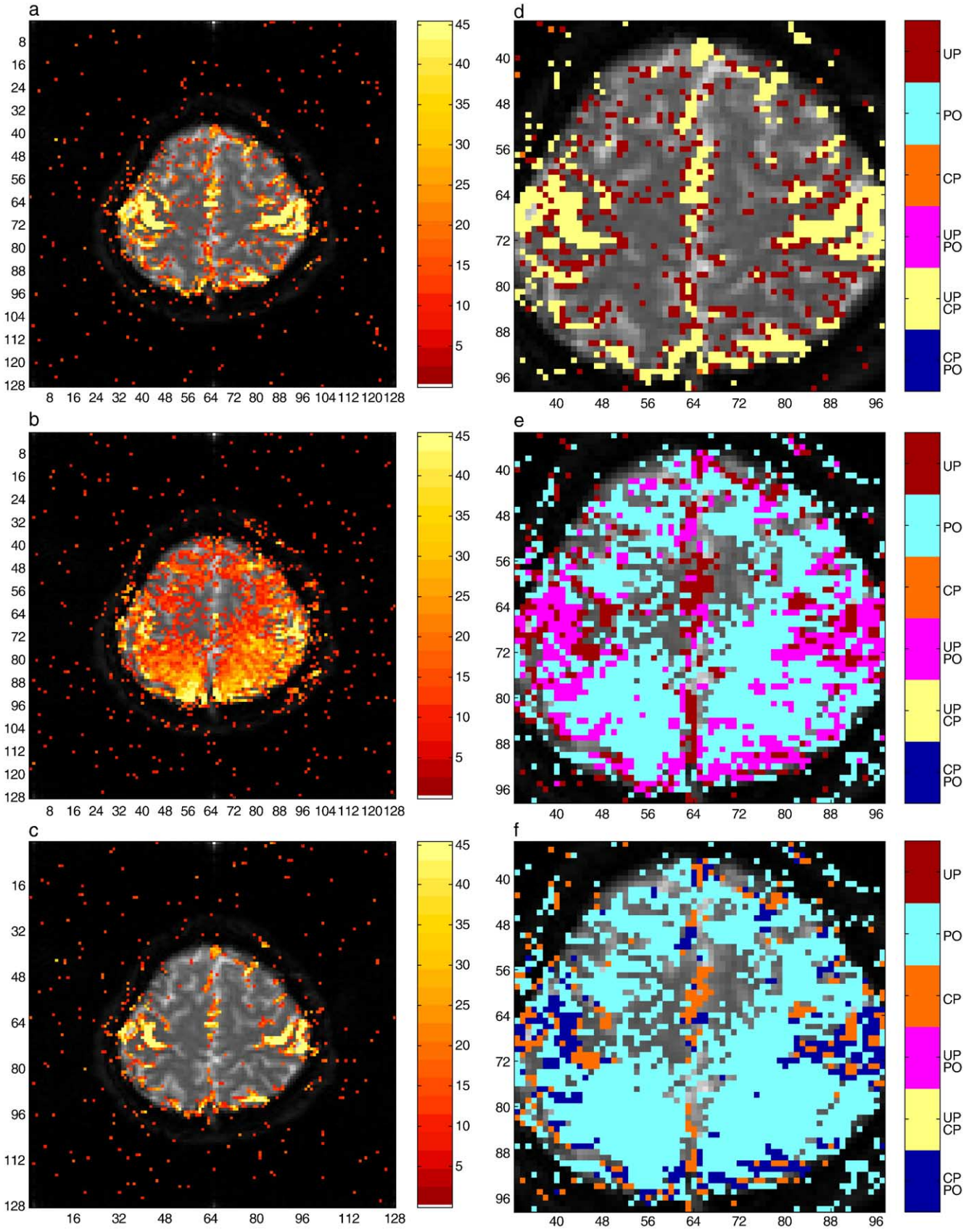

Fig. 3. Thresholded 5% FDR χ^2-statistic activation and overlap maps. (a) Unrestricted phase, (b) phase only, (c) constant phase, (d) overlap map of UP and CP, (e) overlap map of UP and PO, and (f) overlap map of CP and PO.

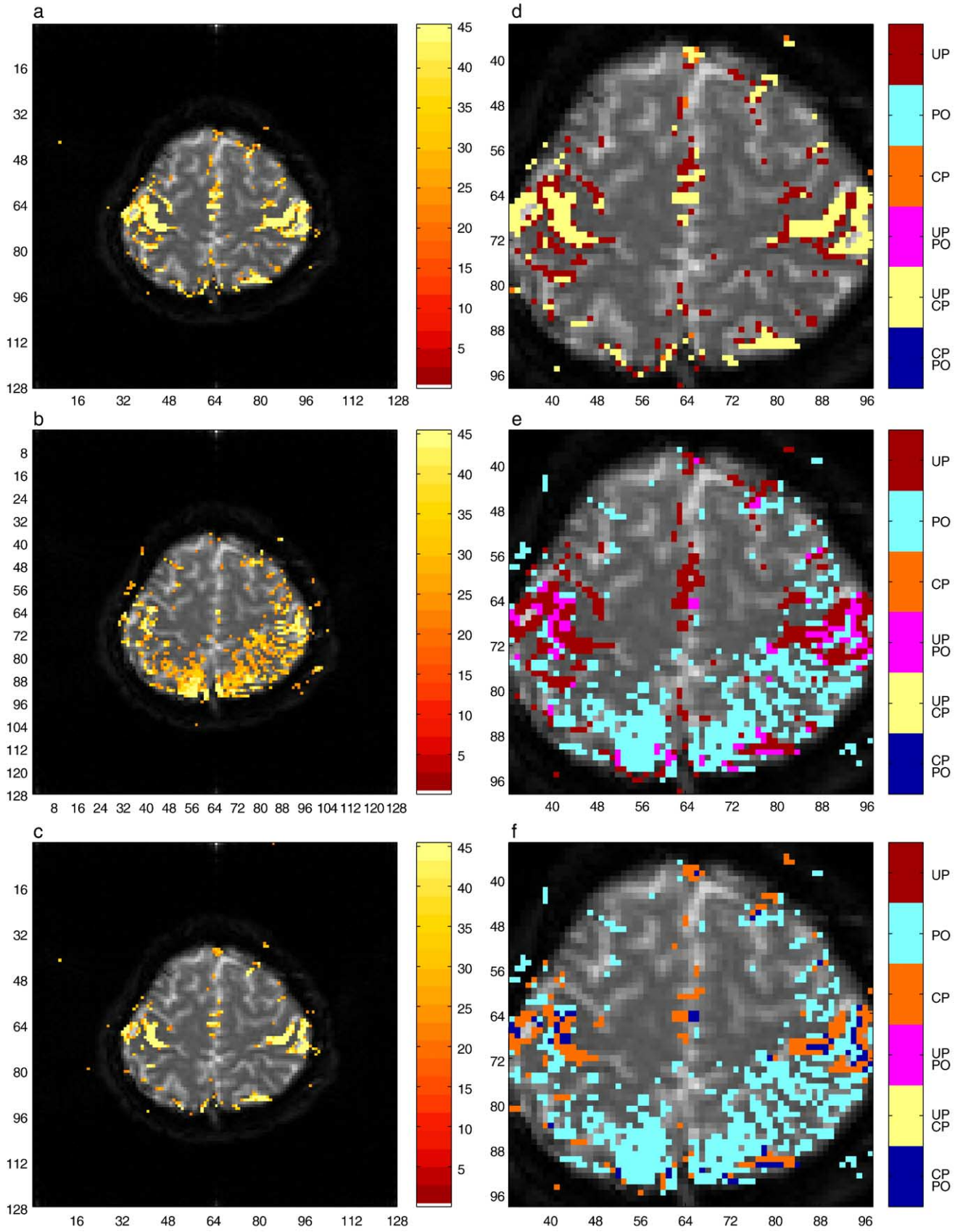

Fig. 4. Thresholded 5% FWE χ^2-statistic activation and overlap maps. (a) Unrestricted phase, (b) phase only, (c) constant phase, (d) overlap map of UP and CP, (e) overlap map of UP and PO, and (f) overlap map of CP and PO.

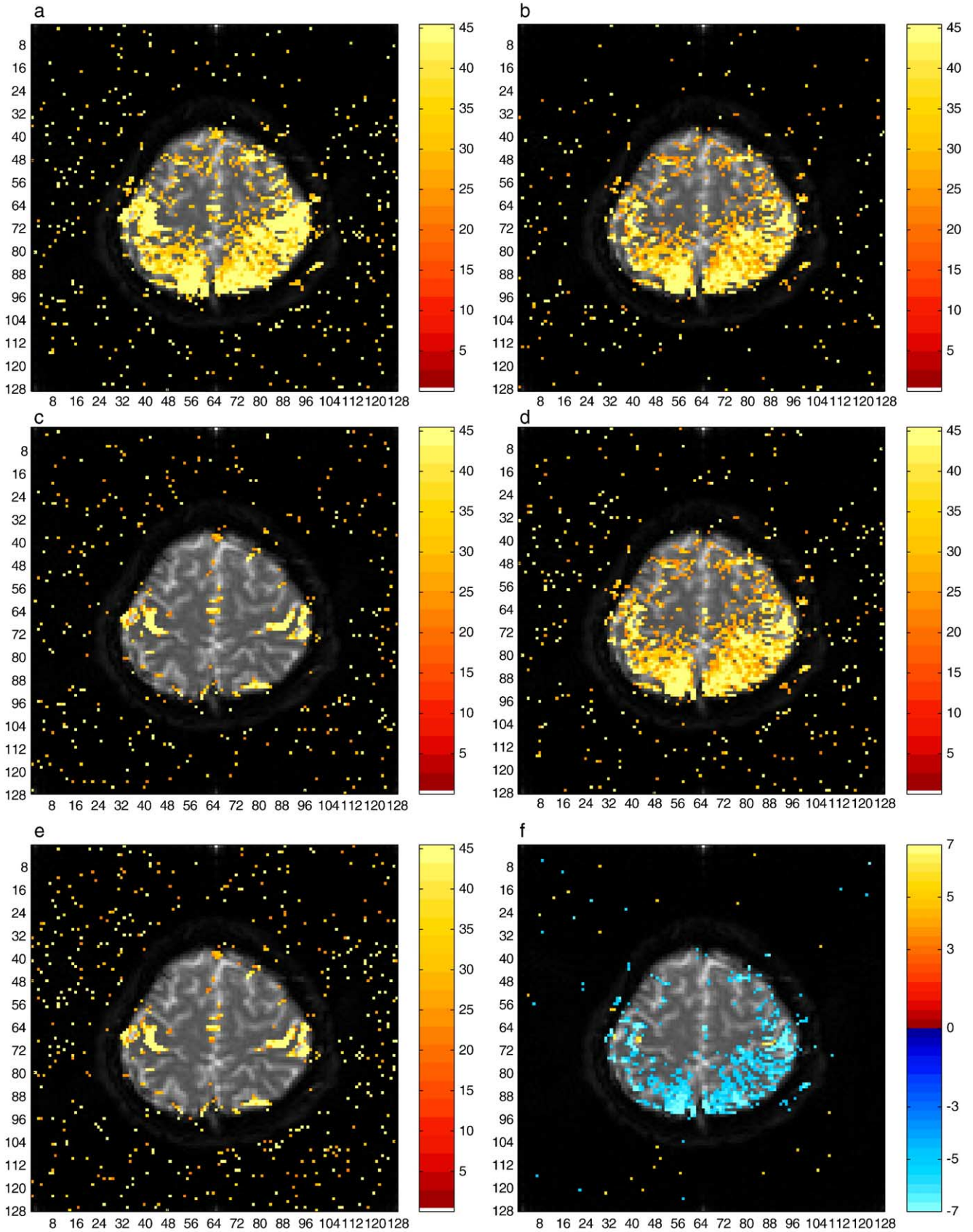

Fig. 5. Thresholded 5% FWE χ^2 -statistic activation and maps. (a) H_d: $C\beta = 0$, $D\gamma = 0$ vs. H_a: $C\beta \neq 0$, $D\gamma \neq 0$; (b) H_d: $C\beta = 0$, $D\gamma = 0$ vs. H_b: $C\beta = 0$, $D\gamma \neq 0$; (c) H_d: $C\beta = 0$, $D\gamma = 0$ vs. H_c: $C\beta \neq 0$, $D\gamma = 0$; (d) H_c: $C\beta \neq 0$, $D\gamma = 0$ vs. H_a: $C\beta \neq 0$, $D\gamma \neq 0$; (e) H_b: $C\beta = 0$, $D\gamma \neq 0$ vs. H_a: $C\beta \neq 0$, $D\gamma \neq 0$; (f) PO t-statistics.

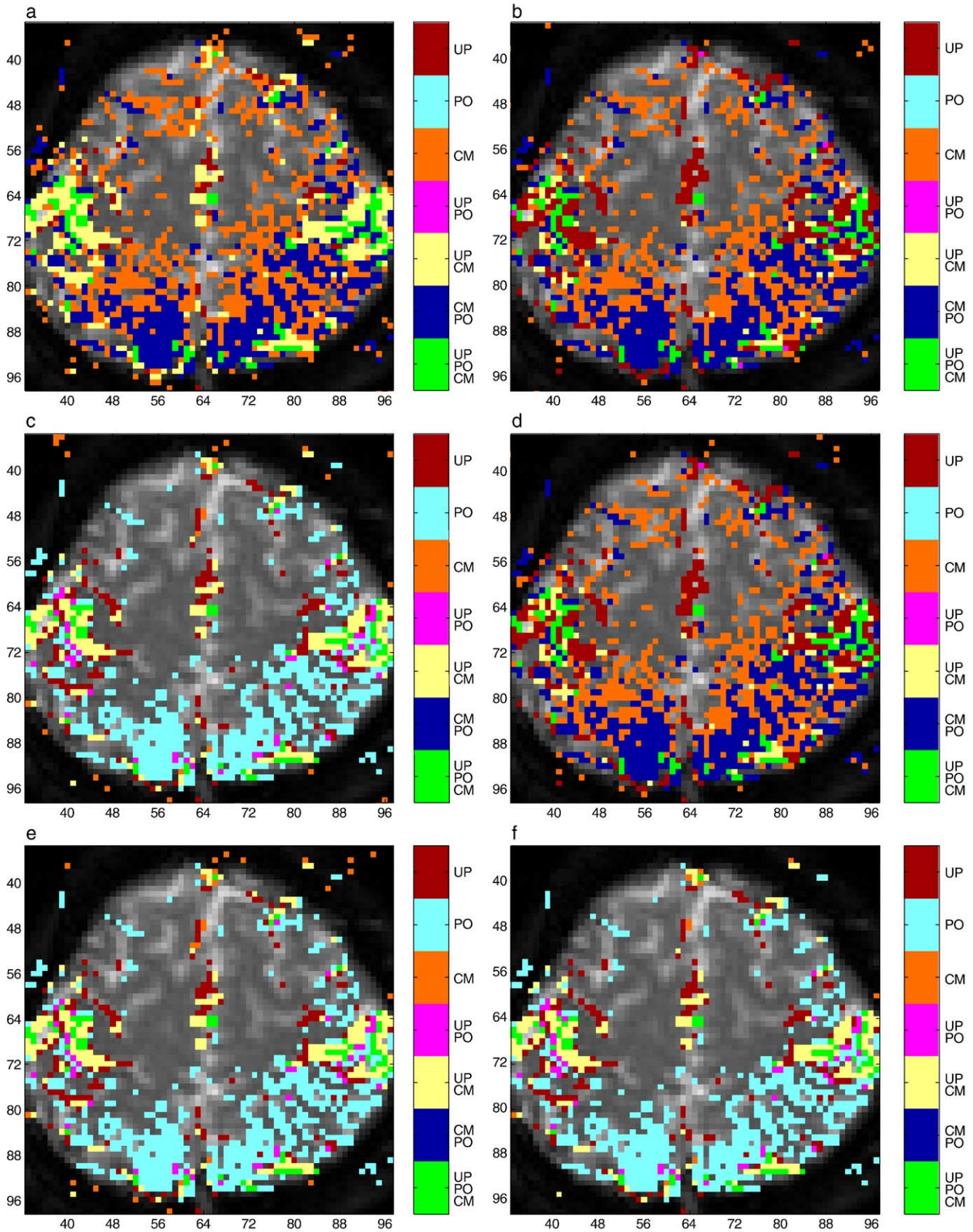

Fig. 6. Thresholded 5% FWE overlap maps. (a) UP, PO, and H_d vs. H_a; (b) UP, PO, and H_d vs. H_b; (c) UP, PO, and H_d vs. H_c; (d) UP, PO, and H_c vs. H_a; (e) UP, PO, and H_b vs. H_a; (f) UP, PO, and CP.

only for the PO model; orange indicates voxels that are above threshold only for the appropriate complex model (CM); light green indicates voxels that are above threshold voxels for all three models, the UP, PO, and the appropriate complex model (CM); yellow indicates voxels that are above the threshold for both the UP and appropriate complex model (CM); dark blue indicates voxels that are above threshold for both the PO and appropriate complex models (CM); pink indicates voxels that are above the threshold for both the UP and PO models; and voxels that were not above threshold for any of the three models retained their anatomical gray scale value.

It can be seen that the overlapping voxel maps from the UP model, the PO model, and CM hypothesis test pairs H_d vs. H_c in Fig. 6c and H_b vs. H_a in Fig. 6e are very similar to the UP, PO, and CP overlap map in Fig. 6f; the overlapping voxel maps from the UP model, the PO model, and the CM hypothesis test pairs H_d vs. H_b in Fig. 6b and H_c vs. H_a in Fig. 6d are very similar to the PO activation map; while the UP model, the PO model, and pair H_d vs. H_a in Fig. 6a appear to be a combined UP and PO overlap map.

Simulated fMRI data

Data are generated to simulate voxel activation from a block design fMRI experiment similar to that of Rowe and Logan (2004) except here, there are six areas of activation that are 5 × 5. The block design consisted of 16 s off followed by eight epochs of 16 s on and 16 s off with an observation interval of 1 s or a TR = 1000 ms. To mimic real data that require magnetic field stabilization, the first three observations were omitted. The simulation consisted of $n = 269$ points where the true activation structure is known to be within the regions of interest (ROIs) so that the models can be evaluated.

Simulated fMRI data are constructed according to the previously described complex time course multiple regression model with a magnitude design matrix $\mathbf{X}$ and a phase design matrix $\mathbf{U}$. The magnitude design matrix is specified to have three columns, the first a column of ones for intercept, the second a column of counting numbers (centered about the mean time) for a linear time trend, and the third a square wave reference function related to a block experimental design. For simplicity, the phase design matrix is taken to be the same as the magnitude design matrix. This model dictates that at time t,

$$y_t = [(\beta_0 + \beta_1 t + \beta_2 x_{2t})\cos(\gamma_0 + \gamma_1 t + \gamma_2 x_{2t}) + \eta_{Rt}] + i[(\beta_0 + \beta_1 t + \beta_2 x_{2t})\sin(\gamma_0 + \gamma_1 t + \gamma_2 x_{2t}) + \eta_{It}], \quad (5.1)$$

where η_{Rt} and η_{It} are i.i.d. $N(0,\sigma^2)$.

In this simulation study, the intercept and observation error standard deviation for all voxels was selected to be $\beta_1 = 0.00001$, and $\sigma = 0.04909$ which are values taken from a highly active voxel (Rowe and Logan, 2004). Therefore, since the variance is held fixed, the SNR within a square 64 × 64 region similar to the brain region in the real data is parameterized by varying β_0 so that the ratio SNR = β_0/σ takes on values 5 and 30, where 30 is approximately the value of SNR found in "highly active" voxels, and smaller values represent decreased SNR. The coefficient for the reference function β_2 within the ROIs has a value determined by a contrast-to-noise ratio (CNR = β_2/σ).

For the simulation, the phase was assigned to follow a linear model $\theta_t = \gamma_0 + \gamma_1 t + \gamma_2 x_{2t}$ or have a task related phase change

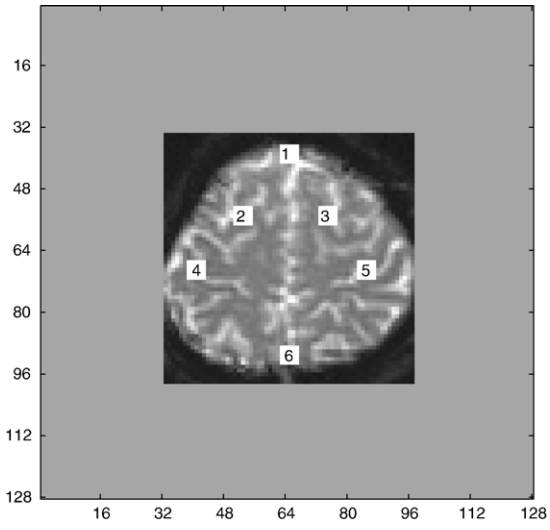

Fig. 7. Anatomical with ROIs.

(TRPC) γ_2. In all voxels $\gamma_0 = \pi/6$, $\gamma_1 = 0.00001$ and for all voxels outside the ~~four~~ six ROIs, $\gamma_2 = 0$. In the ~~five~~ six ROIs lightened in Fig. 7, the (CNR, TRPC) values are in the order of numerically increasing ROIs (1/4, 0), (1/2, π/180), (1/4, π/180), (1/2, π/36), (1/4, π/36), and (0, π/180). The TRPC of π/36 is consistent with previous "large" vessel results (Menon, 2002). Simulated data as just described are generated 1000 times.

In Figs. 8a–c are the 5% Bonferroni FWE detection power maps or percent of the time that the given voxel was above the threshold with simulated data at an SNR = 30 for the (a) complex UP (usual magnitude-only data) model, (b) PO model, (c) the Rowe–Logan complex CP activation model, (d)–(h) the current complex linear regression modeled TRPC activation under five different hypothesis pairs with simulated data at SNR = 30. The same power maps are presented in Fig. 9 except with SNR = 5.

From Figs. 8 and 9, it can be seen that unrestricted phase (magnitude-only data) model detects task related changes in the magnitude regardless of whether or not there is TRPC but is decreased for decreased CNR and the phase-only data model detects task related changes in the phase regardless of whether or not there is task related magnitude changes but is decreased for ROIs with the lower TRPC value when considering the lower SNR value. The Rowe–Logan complex activation model with a constant phase exhibits the same power to detect task related magnitude changes when no TRPC is present. The complex constant phase model exhibits lower power when TRPC is present or biases against voxels with TRPC when the SNR is high.

In the real fMRI data, this biasing property of the complex constant phase model appears to be the reason why voxels were above the Bonferroni FWE threshold for the unrestricted phase model but not for the Rowe–Logan constant phase model. In the real fMRI data, the complex constant phase model biased against voxels that demonstrated TRPC which are potentially ones with large vessels.

It appears to focus on voxels with only task related changes in the magnitude and not those that also demonstrate TRPC unless the CNR is very high such as those in parenchymal tissue. The current complex linear TRPC model was implemented with five hypothesis pairs. The hypothesis pair H_d vs. H_a in Figs. 8d and 9d detects task related activation either in the magnitude, the phase, or both

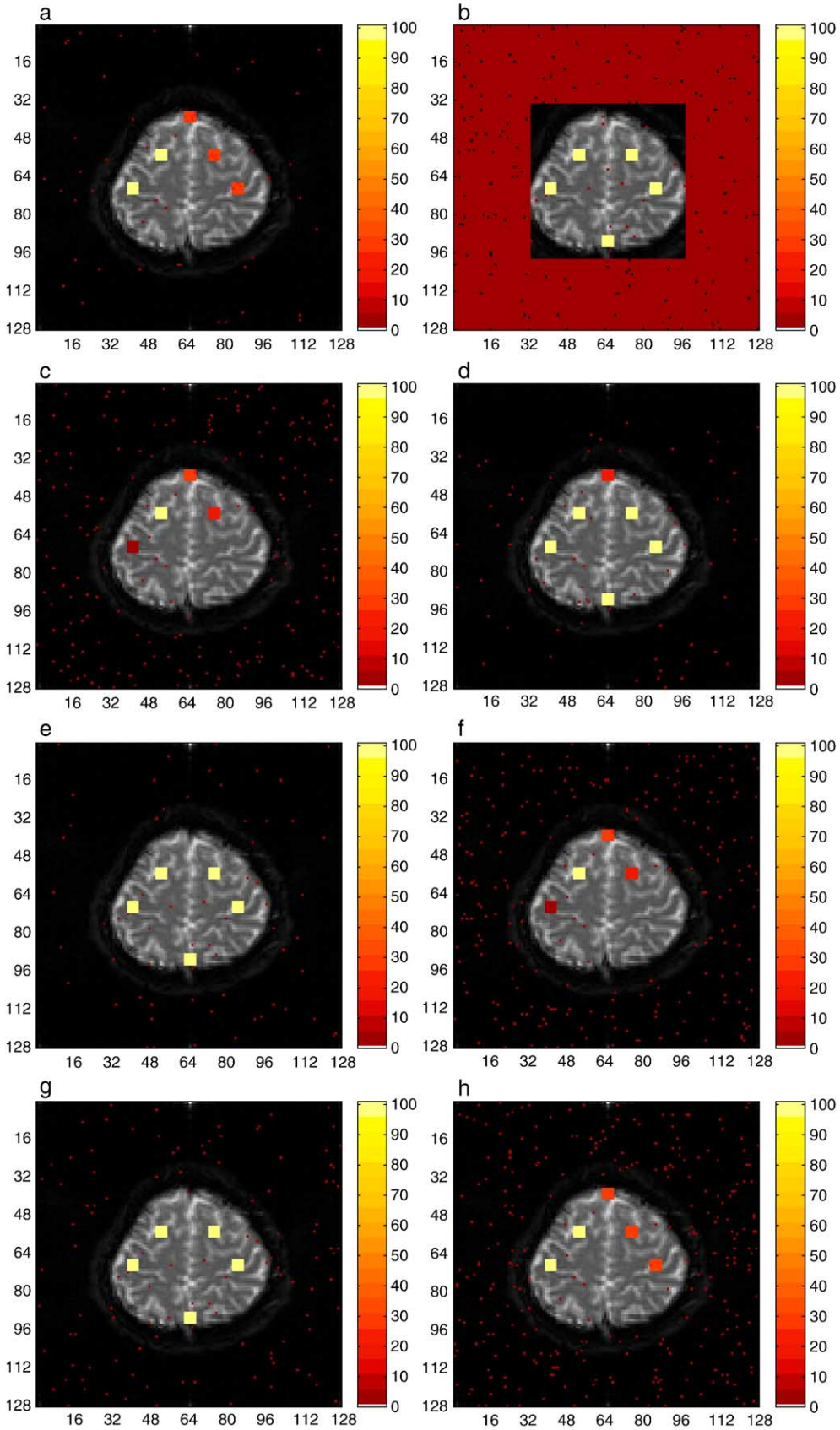

Fig. 8. χ^2-statistic 5% FWE detection power maps SNR = 30. (a) Unrestricted phase; (b) phase only; (c) constant phase; (d) H_d: $C\beta = 0$, $D\gamma = 0$ vs. H_a: $C\beta \neq 0$, $D\gamma \neq 0$; (e) H_d: $C\beta = 0$, $D\gamma = 0$ vs. H_b: $C\beta = 0$, $D\gamma \neq 0$; (f) H_d: $C\beta = 0$, $D\gamma = 0$ vs. H_c: $C\beta \neq 0$, $D\gamma = 0$; (g) H_c: $C\beta \neq 0$, $D\gamma = 0$ vs. H_a: $C\beta \neq 0$, $D\gamma \neq 0$; (h) H_b: $C\beta = 0$, $D\gamma \neq 0$ vs. H_a: $C\beta \neq 0$, $D\gamma \neq 0$.

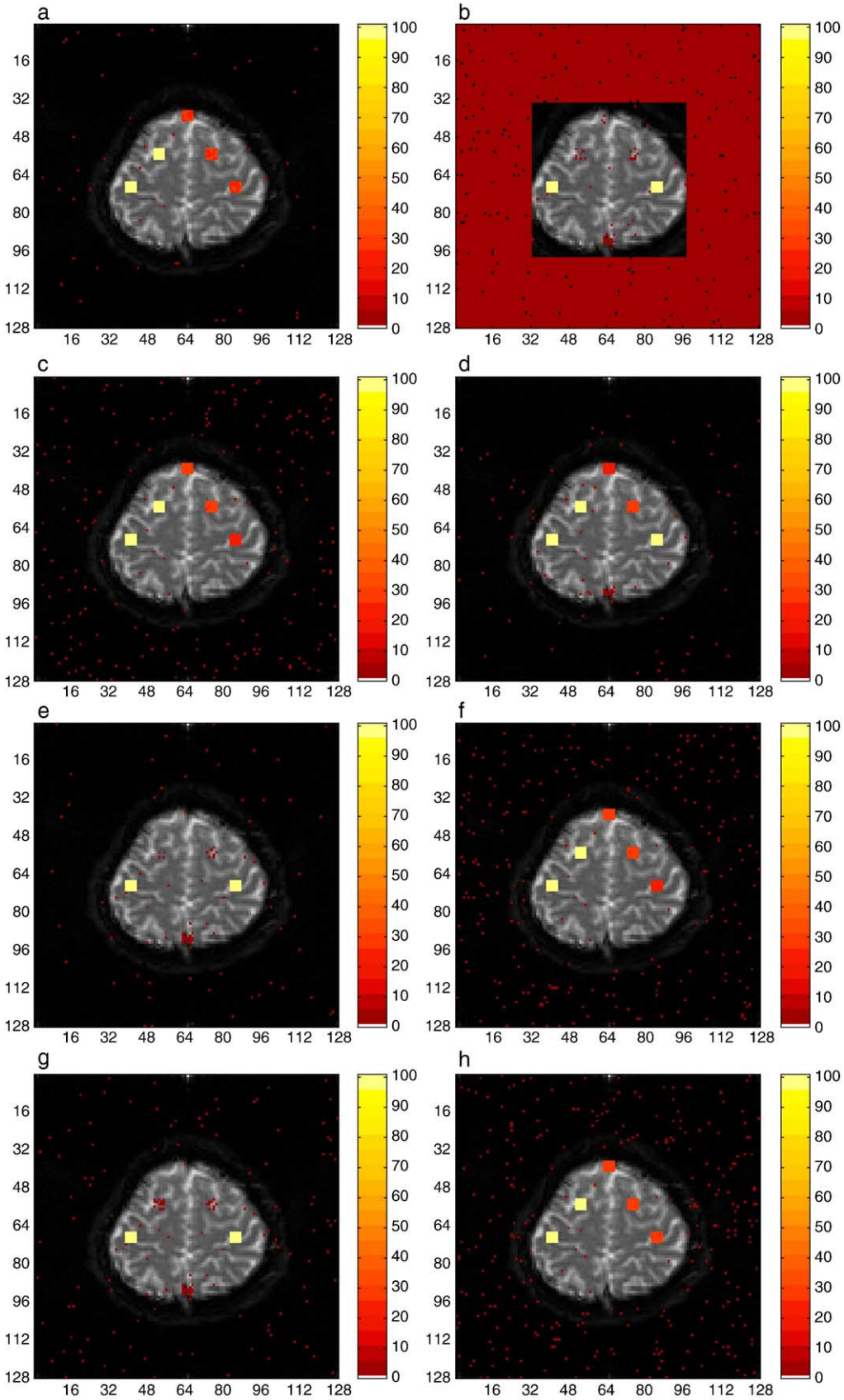

Fig. 9. χ^2-statistic 5% FWE detection power maps SNR = 5. (a) Unrestricted phase; (b) phase only; (c) constant phase; (d) H_d: $C\beta = 0$, $D\gamma = 0$ vs. H_a: $C\beta \neq 0$, $D\gamma \neq 0$; (e) H_d: $C\beta = 0$, $D\gamma = 0$ vs. H_b: $C\beta = 0$, $D\gamma \neq 0$; (f) H_d: $C\beta = 0$, $D\gamma = 0$ vs. H_c: $C\beta \neq 0$, $D\gamma = 0$; (g) H_c: $C\beta \neq 0$, $D\gamma = 0$ vs. H_a: $C\beta \neq 0$, $D\gamma \neq 0$; (h) H_b: $C\beta = 0$, $D\gamma \neq 0$ vs. H_a: $C\beta \neq 0$, $D\gamma \neq 0$.

but has low power regardless of SNR for the low (CNR, TRPC) combination and low phase activation combination; H_d vs. H_b in Figs. 8e and 9e detects task related activation in the phase regardless of whether or not there is task related changes in the magnitude but loses its ability to detect phase activation at the lower SNR; H_d vs. H_c in Figs. 8c and 9c detects task related activation in the magnitude strongly biasing against voxels with TRPC when the SNR is high much like the constant phase model; H_c vs. H_a in Figs. 8g and 9g detects task related activation in the phase regardless of whether or not there is task related changes in the magnitude but loses its ability to detect phase activation at the lower SNR; H_b vs. H_a in Figs. 8h and 9h detects task related activation in the magnitude regardless of whether the phase has TRPC and regardless of SNR.

Conclusion

A generalization of the Rowe–Logan complex activation model was developed that specifically allows for modeling task related changes in both the magnitude and phase. Hypotheses regarding task related magnitude and phase changes are evaluated using derived activation statistics. Activation maps were generated on real data and activation power maps on simulated data for the unrestricted phase or magnitude-only data model, a phase-only data model, the Rowe–Logan constant phase model, and five hypothesis pairs of a newly introduced linear phase model. It was found that the magnitude-only data model declares voxels as active regardless of any phase changes, phase-only data model declares voxels as active regardless of any magnitude changes, and the five complex linear phase models were sensitive to different (CNR, TRPC) combinations. The current complex linear phase model is very general and includes all previously introduced activation models as special cases. Perhaps this model will reach its full potential with other experimental data acquisition methods such as flow tagging or steady state free precession.

Acknowledgment

This work was supported in part by NIH R01EB00215.

Appendix A. Generalized likelihood ratio test

Upon converting from rectangular coordinates (y_{Rt}, y_{It}) in Eq. (2.1) to magnitude and phase polar coordinates $(r_t,\ \phi_t)$, the observed data at time point t can be represented as a 2×1 vector instead of as a complex number

$$\begin{pmatrix} r_t\cos\phi_t \\ r_t\sin\phi_t \end{pmatrix} = \begin{pmatrix} \rho_t\cos\theta_t \\ \rho_t\sin\theta_t \end{pmatrix} + \begin{pmatrix} \eta_{Rt} \\ \eta_{It} \end{pmatrix}, \qquad t = 1,\ldots,n$$

where r_t and ϕ_t are the observed magnitude and phase at time t.

With the aforementioned distributional specifications, the joint distribution of the complex or bivariate observation (y_{Rt}, y_{It}) at time t is

$$p\left(y_{Rt}, y_{It}|\rho_t, \theta_t, \sigma^2\right) = \left(2\pi\sigma^2\right)^{-\frac{2}{2}}\exp\left\{-\frac{(y_{Rt}-\rho_t\cos\theta_t)^2+(y_{It}-\rho_t\sin\theta_t)^2}{2\sigma^2}\right\},$$

which upon making the transformation $(y_{Rt}, y_{It}) = (r_t\cos\phi_t, r_t\sin\phi_t)$ from rectangular coordinates to polar coordinates with Jacobian of the transformation $J\ (y_{Rt},\ y_{It} \rightarrow r_t,\ \phi_t) = r_t$ and some algebra is

$$p\left(r_t, \phi_t|\rho_t, \theta_t, \sigma^2\right) = \frac{r_t}{2\pi\sigma^2}\exp\left\{-\frac{r_t^2+\rho_t^2-2r_t\rho_t\cos(\phi_t-\theta_t)}{2\sigma^2}\right\}.$$

Under appropriate restricted hypotheses, the Lagrange constraints $\psi'\ (C\beta-0)$ and $\delta'\ (\mathbf{D}\gamma\ -\ 0)$ need to be added to the logarithm of the likelihood.

Maximizing this likelihood with respect to the parameters is the same as maximizing the logarithm of the likelihood LL with respect to the parameters. With n temporal observations, the logarithm of the likelihood is

$$\begin{aligned} LL =& -n\log(2\pi) - \sum_{t=1}^{n}\log r_t - n\log\sigma^2 - \frac{1}{2\sigma^2} \\ & \times \sum_{t=1}^{n}\left[r_t^2 + (x_t'\,\beta)^2 - 2(x_t'\,\beta)r_t\cos(\phi_t - u_t'\,\gamma)\right] \\ =& -n\log(2\pi) - \sum_{t=1}^{n}\log r_t - n\log\sigma^2 \\ & -\frac{1}{2\sigma^2}\left[(r-\mathbf{X}\beta)'\,(r-\mathbf{X}\beta) + 2(r-\boldsymbol{r}_*)'\,\mathbf{X}\beta\right] \end{aligned} \tag{A.1}$$

where the linear representations of ρ_t and θ_t have been used while r has t^{th} element r_t and r_* has t^{th} element $r_t\cos(\phi_t - u_t'\,\gamma)$.

The likelihood ratio statistics is computed by maximizing the logarithm of the likelihood LL with respect to the parameters in β, γ, and σ^2 under the appropriate null and alternative hypotheses. Denote the maximized values under the null hypothesis by $(\tilde{\beta}, \tilde{\gamma}, \tilde{\sigma^2})$ and those under the alternative hypothesis as $(\hat{\beta}, \hat{\gamma}, \hat{\sigma}^2)$. These maximized values are then substituted into the likelihoods and the ratio taken.

Then, the generalized likelihood ratio is

$$\begin{aligned} \lambda =& \frac{p\left(r, \phi|\tilde{\beta}, \tilde{\gamma}, \tilde{\sigma}^2, \mathbf{X}, \mathbf{U}\right)}{p\left(r, \phi|\hat{\beta}, \hat{\gamma}, \hat{\sigma}^2, \mathbf{X}, \mathbf{U}\right)} \\ =& \frac{(\tilde{\sigma}^2)^{-2n/2}\exp\left\{-\left[(r-\mathbf{X}\tilde{\beta})'\,(r-\mathbf{X}\tilde{\beta}) + 2(r-\tilde{r}_*)'\,\mathbf{X}\tilde{\beta}\right]/(2\tilde{\sigma}^2)\right\}}{(\hat{\sigma}^2)^{-2n/2}\exp\left\{-\left[(r-\mathbf{X}\hat{\beta})'\,(r-\mathbf{X}\hat{\beta}) + 2(r-\hat{r}_*)'\,\mathbf{X}\hat{\beta}\right]/(2\hat{\sigma}^2)\right\}}, \end{aligned} \tag{A.2}$$

and Eq. (3.1) for the GLRT follows.

Appendix B. Hypotheses

With this model, there are four linear hypotheses that can readily be seen and combined pairwise in several different ways to test distinct hypotheses. The parameters are estimated under each of the hypotheses so that pairs of hypotheses can be used in a generalized likelihood ratio test. Let $\mathbf{C}$ and $\mathbf{D}$ be $r_1 \times (q_1 + 1)$ and $r_2 \times (q_2 + 1)$ matrices of full row rank containing the linear hypothesis constraints in the following.

B.1. H_a: $\mathbf{C}\beta \neq 0$, $\mathbf{D}\gamma \neq 0$

For hypothesis a of unrestricted magnitude and phase, the logarithm of the likelihood is differentiated without any

restrictions. Differentiation of the logarithm of the likelihood with respect to the magnitude regression coefficients $\boldsymbol{\beta}$ proceeds as follows

$$\frac{\partial LL}{\partial \boldsymbol{\beta}} = -\frac{1}{2\sigma^2}\frac{\partial}{\partial \boldsymbol{\beta}}\left[(r-\mathbf{X}\boldsymbol{\beta})'\,(r-\mathbf{X}\boldsymbol{\beta}) + 2\left(r-\boldsymbol{r}_*\right)'\,\mathbf{X}\boldsymbol{\beta}\right]$$

$$= -\frac{1}{2\sigma^2}\frac{\partial}{\partial \boldsymbol{\beta}}\left[-2\mathbf{X}'\,r - 2\mathbf{X}'\,\mathbf{X}\boldsymbol{\beta} + 2\mathbf{X}'\,\left(r-\boldsymbol{r}_*\right)\right].$$

By setting this derivative equal to zero, denoting the parameters with hats, and solving, we get the MLE estimator under the unrestricted model given in Eq. (B.3).

Differentiation of the logarithm of the likelihood with respect to the phase regression coefficients $\boldsymbol{\gamma}$ proceeds as follows

$$\frac{\partial LL}{\partial \boldsymbol{\gamma}} = -\frac{1}{2\sigma^2}\frac{\partial}{\partial \boldsymbol{\gamma}} \times \sum_{t=1}^{n}\left[r_t^2 + (x_t'\,\boldsymbol{\beta})^2 - 2(x_t'\,\boldsymbol{\beta})r_t\cos(\phi_t - u_t'\,\boldsymbol{\gamma})\right]$$

$$\approx \frac{1}{\sigma^2}\frac{\partial}{\partial \boldsymbol{\gamma}}\sum_{t=1}^{n} r_t(x_t'\,\boldsymbol{\beta})\left[1-(\phi_t - u_t'\,\boldsymbol{\gamma})/2\right]$$

$$= \frac{1}{\sigma^2}\frac{\partial}{\partial \boldsymbol{\gamma}}\sum_{t=1}^{n}\left[r_t(x_t'\,\boldsymbol{\beta}) - (\phi_{t*} - z_t'\,\boldsymbol{\gamma})/2\right]$$

$$= \frac{1}{\sigma^2}\frac{\partial}{\partial \boldsymbol{\gamma}}\left[r'\,\mathbf{X}\boldsymbol{\beta} - \frac{1}{2}(\phi_* - \mathbf{Z}\boldsymbol{\gamma})'\,(\phi_* - \mathbf{Z}\boldsymbol{\gamma})\right]$$

$$= \frac{1}{\sigma^2}\left[-2\mathbf{Z}'\,\phi_* + 2\mathbf{Z}'\,\mathbf{Z}\boldsymbol{\gamma}\right]$$

where $\hat{\boldsymbol{\phi}}_*$ is an $n \times 1$ vector with t^{th} element $\phi_{t*} = \phi_t\sqrt{r_t x_t'\,\boldsymbol{\beta}}$, and $\mathbf{Z}$ is an $n \times (q_2+1)$ matrix with t^{th} row $z_t' = u_t'\sqrt{r_t(x_t'\,\boldsymbol{\beta})}$. By setting this derivative equal to zero, denoting the parameters with hats, and solving, we get the MLE estimator in Eq. (B.3). Note that a Taylor series approximation to the cosine was used. This approximation is robust to a mild difference in its argument $\alpha = \phi_t - u_t'\boldsymbol{\gamma}$. For example, if $\alpha = \pi/12$ radians or 15 degrees, the exact cosine is 0.9659 while the approximation yields 0.9657. Results from previous literature (Menon, 2002) find that the phase may deviate from its mean by as much as 5 degrees in voxels with large vessels. Note that the same result is found by differentiating the cosine exactly and approximating the resulting sinusoid,

$$\frac{\partial}{\partial \boldsymbol{\gamma}}\cos(\phi_t - u_t'\,\boldsymbol{\gamma}) = -u_t\sin(\phi_t - u_t'\,\boldsymbol{\gamma}) \approx -u_t(\phi_t - u_t'\,\boldsymbol{\gamma}).$$

Differentiation of the logarithm of the likelihood with respect to the variance σ^2 proceeds as follows

$$\frac{\partial LL}{\partial \sigma^2} = -n\left(\sigma^2\right)^{-1} - \frac{1}{2}\left[(r-\mathbf{X}\boldsymbol{\beta})'\,(r-\mathbf{X}\boldsymbol{\beta}) + 2\left(r-\boldsymbol{r}_*\right)'\,\mathbf{X}\boldsymbol{\beta}\right](\sigma^2)^{-2}.$$

By setting this derivative equal to zero, denoting the parameters with hats, and solving, we get the MLE under the unrestricted model given in Eq. (B.3).

The maximum likelihood estimators under this hypothesis are given by

$$\hat{\beta} = (\mathbf{X}'\,\mathbf{X})^{-1}\mathbf{X}'\,\hat{r}_*$$

$$\hat{\boldsymbol{\gamma}} = \left(\hat{\mathbf{Z}}'\,\hat{\mathbf{Z}}\right)^{-1}\hat{\mathbf{Z}}\hat{\phi}_*$$

$$\hat{\sigma}^2 = \frac{1}{2n}\left[(r-\mathbf{X}\hat{\boldsymbol{\beta}})'\,\left(r-\mathbf{X}\hat{\boldsymbol{\beta}}\right) + 2\left(r-\hat{\boldsymbol{r}}_*\right)'\,\mathbf{X}\hat{\boldsymbol{\beta}}\right], \tag{B.3}$$

where $\hat{\boldsymbol{r}}_*$ is an $n \times 1$ vector with t^{th} element $r_t\cos(\phi_t - u_t'\,\hat{\gamma})$, $\hat{\boldsymbol{Z}}$ is an $n \times (q_2+1)$ matrix with t^{th} $\underline{\text{row}}\ \hat{z}_t' = u_t'\sqrt{r_t x_t'\,\hat{\boldsymbol{\beta}}}$, $\boldsymbol{\phi}_*$ is an $n \times 1$ vector with t^{th} element $\phi_t\sqrt{r_t x_t'\,\hat{\boldsymbol{\beta}}}$, and $\boldsymbol{r}$ is an $n \times 1$ vector of observed magnitudes. In deriving the MLE $\hat{\boldsymbol{\gamma}}$, an approximation was made for a cosine term.

B.2. H_b: $\mathbf{C}\beta = 0$, $\mathbf{D}\gamma \neq 0$

For hypothesis b of restricted magnitude but not phase, the logarithm of the likelihood is differentiated with the added Lagrange restriction $\Psi'\ (\mathbf{C}\beta - 0)$. Differentiation of the logarithm of the likelihood that includes the Lagrange constraint with respect to the magnitude regression coefficients $\boldsymbol{\beta}$ proceeds as follows

$$\frac{\partial LL}{\partial \boldsymbol{\beta}} = \frac{\partial}{\partial \boldsymbol{\beta}}\left\{\frac{1}{2\sigma^2}\left[(r-\mathbf{X}\boldsymbol{\beta})'(r-\mathbf{X}\boldsymbol{\beta}) + 2(r-\boldsymbol{r}_*)'\,\mathbf{X}\boldsymbol{\beta}\right] + \psi'(\mathbf{C}\boldsymbol{\beta} - 0)\right\}$$

$$= -\frac{1}{2\sigma^2}\left[-2\mathbf{X}'\,r - 2\mathbf{X}'\,\mathbf{X}\boldsymbol{\beta} + 2\mathbf{X}'\,\left(r-\boldsymbol{r}_*\right)\right] + \mathbf{C}'\,\psi$$

where the variables are as previously defined. By setting this derivative equal to zero, denoting the parameters with breves, and solving, we get the MLE estimator in Eq. (B.4) below.

Differentiation of the logarithm of the likelihood with respect to the phase regression coefficients $\boldsymbol{\gamma}$ proceeds as follows

$$\frac{\partial LL}{\partial \boldsymbol{\gamma}} = -\frac{\partial}{\partial \boldsymbol{\gamma}}\left\{\frac{1}{2\sigma^2}\sum_{t=1}^{n}\left[r_t^2 + (x_t'\,\boldsymbol{\beta})^2 - 2(x_t'\,\boldsymbol{\beta})r_t\cos(\phi_t - u_t'\,\boldsymbol{\gamma})\right]\right\}$$

$$\approx \frac{\partial}{\partial \boldsymbol{\gamma}}\left\{\frac{1}{2\sigma^2}\sum_{t=1}^{n} r_t(x_t'\,\boldsymbol{\beta})[1-(\phi_t - u_t'\,\boldsymbol{\gamma})/2]\right\}$$

$$= \frac{\partial}{\partial \boldsymbol{\gamma}}\left\{\frac{1}{2\sigma^2}\sum_{t=1}^{n}[r_t(x_t'\,\boldsymbol{\beta}) - (\phi_{t*} - z_t'\,\boldsymbol{\gamma})/2]\right\}$$

$$= \frac{\partial}{\partial \boldsymbol{\gamma}}\left\{\frac{1}{2\sigma^2}\left[r'\,\mathbf{X}\boldsymbol{\beta} - \frac{1}{2}(\phi_* - \mathbf{Z}\boldsymbol{\gamma})'\,(\phi_* - \mathbf{Z}\boldsymbol{\gamma})\right]\right\}$$

$$= \frac{1}{2\sigma^2}[-2\mathbf{Z}'\,\phi_* + 2\mathbf{Z}'\,\mathbf{Z}\boldsymbol{\gamma}]$$

where the variables are as previously defined. By setting this derivative equal to zero, denoting the parameters with breves, and solving, we get the MLE estimator in Eq. (B.4) below.

Differentiation of the logarithm of the likelihood with respect to the variance σ^2 proceeds as follows

$$\frac{\partial LL}{\partial \sigma^2} = -n(\sigma^2)^{-1} - \frac{1}{2}[(r-\mathbf{X}\boldsymbol{\beta})'(r-\mathbf{X}\boldsymbol{\beta}) + 2(r-r_*)'\mathbf{X}\boldsymbol{\beta}](\sigma^2)^{-2}.$$

By setting this derivative equal to zero, denoting the parameters with breves, and solving, we get the MLE under the unrestricted model given in Eq. (B.4) below.

The maximum likelihood estimators under this hypothesis are given by

$$\breve{\boldsymbol{\beta}} = \Psi(\mathbf{X}'\mathbf{X})^{-1}\mathbf{X}'\breve{\boldsymbol{r}}_*$$

$$\breve{\boldsymbol{\gamma}} = (\breve{\mathbf{Z}}'\breve{\mathbf{Z}})^{-1}\breve{\mathbf{Z}}'\breve{\boldsymbol{\phi}}_*$$

$$\breve{\sigma}^2 = \frac{1}{2n}[(r-\mathbf{X}\breve{\boldsymbol{\beta}})'(r-\mathbf{X}\breve{\boldsymbol{\beta}}) + 2(r-\breve{\boldsymbol{r}}_*)'\mathbf{X}\breve{\boldsymbol{\beta}}]$$

$$\Psi = I_{q_1+1} - (\mathbf{X}'\mathbf{X})^{-1}\mathbf{C}'\left[\mathbf{C}(\mathbf{X}'\mathbf{X})^{-1}\mathbf{C}'\right]^{-1}\mathbf{C}, \tag{B.4}$$

where $\breve{\boldsymbol{r}}_*$ is an $n \times 1$ vector with t^{th} element $\breve{\mathbf{r}}_t \cos(\phi_t - u_t'\breve{\boldsymbol{\gamma}})$, $\breve{\mathbf{Z}}$ is an $n \times (q_2+1)$ matrix with t^{th} row $\breve{z}_t' = u_t'\sqrt{r_t x_t'\breve{\boldsymbol{\beta}}}$, $\breve{\boldsymbol{\phi}}_*$ is an $n \times 1$ vector with t^{th} element $\phi_t\sqrt{r_t x_t'\breve{\boldsymbol{\beta}}}$, and r is as above. In computing maximum likelihood estimates, an iterative maximization algorithm (Lindley and Smith, 1972; Rowe, 2001, 2003) is used.

B.3. H_c: $\mathbf{C}\beta \neq 0$, $\mathbf{D}\gamma = 0$

For hypothesis c of restricted phase but not magnitude, the logarithm of the likelihood is differentiated with the added Lagrange restrictions $\delta'(\mathbf{D}\gamma - 0)$. Differentiation of the logarithm of the likelihood that includes the Lagrange constraints with respect to the phase regression coefficients $\boldsymbol{\beta}$ proceeds as follows

$$\frac{\partial LL}{\partial \boldsymbol{\beta}} = \frac{\partial}{\partial \boldsymbol{\beta}}\left\{\frac{1}{2\sigma^2}[(r-\mathbf{X}\boldsymbol{\beta})'(r-\mathbf{X}\boldsymbol{\beta}) + 2(r-\boldsymbol{r}_*)'\mathbf{X}\boldsymbol{\beta}] + \delta'(\mathbf{D}\boldsymbol{\gamma} - 0)\right\}$$

$$= -\frac{1}{2\sigma^2}[-2\mathbf{X}'r - 2\mathbf{X}'\mathbf{X}\boldsymbol{\beta} + 2\mathbf{X}'(r-\boldsymbol{r}_*)]$$

where the variables are as previously defined. By setting this derivative equal to zero, denoting the parameters with breves, and solving, we get the MLE estimator in Eq. (B.4) below.

Differentiation of the logarithm of the likelihood that includes the Lagrange contraints with respect to the phase regression coefficients $\boldsymbol{\gamma}$ proceeds as follows

$$\frac{\partial LL}{\partial \boldsymbol{\gamma}} = -\frac{\partial}{\partial \boldsymbol{\gamma}}\left\{\frac{1}{2\sigma^2}\sum_{t=1}^{n}\left[r_t^2 + (x_t'\boldsymbol{\beta})^2 - 2(x_t'\boldsymbol{\beta})r_t\cos(\phi_t - u_t'\boldsymbol{\gamma})\right] + \delta'(\mathbf{D}\boldsymbol{\gamma} - 0)\right\}$$

$$\approx \frac{\partial}{\partial \boldsymbol{\gamma}}\left\{\frac{1}{2\sigma^2}\sum_{t=1}^{n} r_t(x_t'\boldsymbol{\beta})[1 - (\phi_t - u_t'\boldsymbol{\gamma})/2] + \delta'\mathbf{D}\boldsymbol{\gamma}\right\}$$

$$= \frac{\partial}{\partial \boldsymbol{\gamma}}\left\{\frac{1}{2\sigma^2}\sum_{t=1}^{n}[r_t(x_t'\boldsymbol{\beta}) - (\phi_{t*} - z_t'\boldsymbol{\gamma})/2] + \delta'\mathbf{D}\boldsymbol{\gamma}\right\}$$

$$= \frac{\partial}{\partial \boldsymbol{\gamma}}\left\{\frac{1}{2\sigma^2}\left[r'\mathbf{X}\boldsymbol{\beta} - \frac{1}{2}(\boldsymbol{\phi}_* - \mathbf{Z}\boldsymbol{\gamma})'(\boldsymbol{\phi}_* - \mathbf{Z}\boldsymbol{\gamma})\right] + \delta'\mathbf{D}\right\}$$

$$= \frac{1}{2\sigma^2}[-2\mathbf{Z}'\boldsymbol{\phi}_* + 2\mathbf{Z}'\mathbf{Z}\boldsymbol{\gamma}] + \delta'\mathbf{D}\boldsymbol{\gamma}$$

where the variables are as previously defined. By setting this derivative equal to zero, denoting the parameters with bars, and solving, we get the MLE estimator in Eq. (B.5) below.

Differentiation of the logarithm of the likelihood with respect to the variance σ^2 proceeds as follows

$$\frac{\partial LL}{\partial \sigma^2} = -n(\sigma^2)^{-1} - \frac{1}{2}[(r-\mathbf{X}\boldsymbol{\beta})'(r-\mathbf{X}\boldsymbol{\beta}) + 2(r-r_*)'\mathbf{X}\boldsymbol{\beta}](\sigma^2)^{-2}.$$

By setting this derivative equal to zero, denoting the parameters with bars, and solving, we get the MLE under the unrestricted model given in Eq. (B.5) below.

The maximum likelihood estimators under this hypothesis are given by

$$\bar{\boldsymbol{\beta}} = (\mathbf{X}'\mathbf{X})^{-1}\mathbf{X}'\bar{\boldsymbol{r}}_*$$

$$\bar{\boldsymbol{\gamma}} = \Omega(\bar{\mathbf{Z}}'\bar{\mathbf{Z}})^{-1}\bar{\mathbf{Z}}'\bar{\boldsymbol{\phi}}_*$$

$$\bar{\sigma}^2 = \frac{1}{2n}[(r-\mathbf{X}\bar{\boldsymbol{\beta}})'(r-\mathbf{X}\bar{\boldsymbol{\beta}}) + 2(r-\bar{\boldsymbol{r}}_*)'\mathbf{X}\bar{\boldsymbol{\beta}}]$$

$$\Omega = I_{q_2+1} - (\bar{\mathbf{Z}}'\bar{\mathbf{Z}})^{-1}\mathbf{D}'[\mathbf{D}(\bar{\mathbf{Z}}'\bar{\mathbf{Z}})^{-1}\mathbf{D}']^{-1}\mathbf{D}, \tag{B.5}$$

where $\bar{\boldsymbol{r}}_*$ is an $n \times 1$ vector with t^{th} element $\bar{\boldsymbol{r}}_t \cos(\phi_t - u_t'\bar{\boldsymbol{\gamma}})$, $\bar{\mathbf{Z}}$ is an $n \times (q_2+1)$ matrix with t^{th} row $\bar{z}_t' = u_t'\sqrt{r_t x_t'\bar{\boldsymbol{\beta}}}$, $\bar{\boldsymbol{\phi}}_*$ is an $n \times 1$ vector with t^{th} element $\bar{\phi}_t\sqrt{r_t x_t'\bar{\boldsymbol{\beta}}}$, and r is as above. In computing maximum likelihood estimates, an iterative maximization algorithm is used (Lindley and Smith, 1972; Rowe, 2001, 2003).

B.4. H_d: $\mathbf{C}\beta = 0$, $\mathbf{D}\gamma = 0$

For hypothesis d of linearly restricted magnitude and phase, the logarithm of the likelihood is differentiated with the added Lagrange restrictions $\psi'(\mathbf{C}\beta - 0)$ and $\delta'(\mathbf{D}\gamma - 0)$. Differentiation of the logarithm of the likelihood that includes the Lagrange constraints with respect to the magnitude regression coefficients $\boldsymbol{\beta}$ proceeds as follows

$$\frac{\partial LL}{\partial \boldsymbol{\beta}} = \frac{\partial}{\partial \boldsymbol{\beta}}\left\{\frac{1}{2\sigma^2}[(r-\mathbf{X}\boldsymbol{\beta})'(r-\mathbf{X}\boldsymbol{\beta}) + 2(r-\boldsymbol{r}_*)'\mathbf{X}\boldsymbol{\beta}] + \psi'(\mathbf{C}\boldsymbol{\beta} - 0) + \delta'(\mathbf{D}\boldsymbol{\gamma} - 0)\right\}$$

$$= -\frac{1}{2\sigma^2}[-2\mathbf{X}'r - 2\mathbf{X}'\mathbf{X}\boldsymbol{\beta} + 2\mathbf{X}'(r-\boldsymbol{r}_*)] + \mathbf{C}'\psi$$

where the variables are as previously defined. By setting this derivative equal to zero, denoting the parameters with tildes, and solving, we get the MLE estimator in Eq. (B.6).

Differentiation of the logarithm of the likelihood that includes the Lagrange constraints with respect to the phase regression coefficients $\boldsymbol{\gamma}$ proceeds as follows

$$\begin{aligned}\frac{\partial LL}{\partial \boldsymbol{\gamma}} &= -\frac{\partial}{\partial \boldsymbol{\gamma}}\left\{\frac{1}{2\sigma^2}\sum_{t=1}^{n}\left[r_t^2+(x_t'\,\boldsymbol{\beta})^2-2(x_t'\,\boldsymbol{\beta})r_t\cos(\phi_t-u_t'\,\boldsymbol{\gamma})\right]\right.\\ &\qquad\left.+\;\boldsymbol{\psi}'\,(C\boldsymbol{\beta}-0)+\boldsymbol{\delta}'\,(\mathbf{D}\boldsymbol{\gamma}-0)\right\}\\ &\approx \frac{\partial}{\partial \boldsymbol{\gamma}}\left\{\frac{1}{2\sigma^2}\sum_{t=1}^{n}r_t(x_t'\,\boldsymbol{\beta})[1-(\phi_t-u_t'\,\boldsymbol{\gamma})/2]+\boldsymbol{\delta}'\,\mathbf{D}\boldsymbol{\gamma}\right\}\\ &= \frac{\partial}{\partial \boldsymbol{\gamma}}\left\{\frac{1}{2\sigma^2}\sum_{t=1}^{n}[r_t(x_t'\,\boldsymbol{\beta})-(\phi_{t*}-z_t'\,\boldsymbol{\gamma})/2]+\boldsymbol{\delta}'\,\mathbf{D}\boldsymbol{\gamma}\right\}\\ &= \frac{\partial}{\partial \boldsymbol{\gamma}}\left\{\frac{1}{2\sigma^2}\left[r'\,\mathbf{X}\boldsymbol{\beta}-\frac{1}{2}(\boldsymbol{\phi}_*-\mathbf{Z}\boldsymbol{\gamma})'\,(\boldsymbol{\phi}_*-\mathbf{Z}\boldsymbol{\gamma})\right]+\boldsymbol{\delta}'\,\mathbf{D}\boldsymbol{\gamma}\right\}\\ &= \frac{1}{2\sigma^2}[-2\mathbf{Z}'\,\boldsymbol{\phi}_*+2\mathbf{Z}'\,\mathbf{Z}\boldsymbol{\gamma}]+\mathbf{D}'\,\boldsymbol{\delta}\end{aligned}$$

where the variables are as previously defined. By setting this derivative equal to zero, denoting the parameters with tildes, and solving, we get the MLE estimator in Eq. (B.6).

Differentiation of the logarithm of the likelihood with respect to the variance σ^2 proceeds as follows

$$\begin{aligned}\frac{\partial LL}{\partial \sigma^2} &= -n\left(\sigma^2\right)^{-1}\\ &\quad-\frac{1}{2}\left[(r-\mathbf{X}\boldsymbol{\beta})'\,(r-\mathbf{X}\boldsymbol{\beta})+2\left(r-\boldsymbol{r}_*\right)'\,\mathbf{X}\boldsymbol{\beta}\right]\left(\sigma^2\right)^{-2}.\end{aligned}$$

By setting this derivative equal to zero, denoting the parameters with tildes, and solving, we get the MLEs under the unrestricted model given in Eq. (B.6) below.

The maximum likelihood estimators under this hypothesis are given by

$$\begin{aligned}\tilde{\boldsymbol{\beta}} &= \Psi(\mathbf{X}'\,\mathbf{X})^{-1}\mathbf{X}'\,\tilde{\boldsymbol{r}}_*\\ \tilde{\boldsymbol{\gamma}} &= \Omega\left(\tilde{\mathbf{Z}}'\,\tilde{\mathbf{Z}}\right)^{-1}\tilde{\mathbf{Z}}'\,\tilde{\phi}_*\\ \tilde{\sigma}^2 &= \frac{1}{2n}\left[\left(r-\mathbf{X}\tilde{\boldsymbol{\beta}}\right)'\,\left(r-\mathbf{X}\tilde{\boldsymbol{\beta}}\right)+2\left(r-\tilde{\boldsymbol{r}}_*\right)'\,\mathbf{X}\tilde{\boldsymbol{\beta}}\right]\\ \Psi &= I_{q_1+1}-(\mathbf{X}'\,\mathbf{X})^{-1}\mathbf{C}'\,\left[\mathbf{C}(\mathbf{X}'\,\mathbf{X})^{-1}\mathbf{C}'\right]^{-1}\mathbf{C}\\ \Omega &= I_{q_2+1}-\left(\tilde{\mathbf{Z}}'\,\tilde{\mathbf{Z}}\right)^{-1}\mathbf{D}'\,\left[\mathbf{D}\left(\tilde{\mathbf{Z}}'\,\tilde{\mathbf{Z}}\right)^{-1}\mathbf{D}'\right]^{-1}\mathbf{D},\end{aligned}\qquad\text{(B.6)}$$

where $\tilde{\boldsymbol{r}}_*$ is an $n\times 1$ vector with t^{th} element $\tilde{\boldsymbol{r}}_t\cos(\phi_t-u_t'\,\tilde{\gamma})$, $\tilde{\mathbf{Z}}$ is an $n\times(q_2+1)$ matrix with t^{th} row $\tilde{z}_t'=u_t'\sqrt{r_tx_t'\,\tilde{\boldsymbol{\beta}}}$, $\tilde{\phi}_*$ is an $n\times 1$ vector with t^{th} element $\phi_t\sqrt{r_tx_t'\,\tilde{\boldsymbol{\beta}}}$, and r is as above. In computing maximum likelihood estimates under both hypotheses, an iterative maximization algorithm is used (Lindley and Smith, 1972; Rowe, 2001, 2003).

References

Bandettini, P., Jesmanowicz, A., Wong, E., Hyde, J.S., 1993. Processing strategies for time-course data sets in functional MRI of the human brain. Magn. Reson. Med. 30 (2), 161–173.

Bernstein, M.A., Thomasson, D.M., Perman, W.H., 1989. Improved detectability in low signal-to-noise ratio magnetic resonance images by means of a phase-corrected real reconstruction. Med. Phys. 16 (5), 813–817.

Cox, R.W., Jesmanowicz, A., Hyde, J.S., 1995. Real-time functional magnetic resonance imaging. Magn. Reson. Med. 33 (2), 230–236.

Gonzales, R.C., Woods, R.E., 1992. Digital Image Processing. Addison-Wesley Publishing Company, Reading, Massachusetts.

Gudbjartsson, H., Patz, S., 1995. The Rician distribution of noisy data. Magn. Reson. Med. 34 (6), 910–914.

Haacke, E.M., Brown, R., Thompson, M., Venkatesan, R., 1999. Magnetic Resonance Imaging: Principles and Sequence Design. John Wiley and Sons, New York, NY, USA.

Hoogenrad, F.G., Reichenbach, J.R., Haacke, E.M., Lai, S., Kuppusamy, K., Sprenger, M., 1998. In vivo measurement of changes in venous blood-oxygenation with high resolution functional MRI at .95 Tesla by measuring changes in susceptibility and velocity. Magn. Reson. Med. 39 (1), 97–107.

Lindley, D.V., Smith, A.F.M., 1972. Bayes estimates for the linear model. J. R. Stat. Soc., B 34, 1.

Logan, B.R., Rowe, D.B., 2004. An evaluation of thresholding techniques in fMRI analysis. NeuroImage 22 (1), 95–108.

Macovski, A., 1996. Noise in MRI. Magn. Reson. Med. 36 (3), 494–497.

Menon, R.S., 2002. Postacquisition suppression of large-vessel BOLD signals in high-resolution fMRI. Magn. Reson. Med. 47(1):1–9. Magn. Reson. Med. 47 (1), 1–9.

Press, W.H., Teukolsky, S.A., Vetterling, W.T., Flannery, B.P., 1992. Numerical Recipies in C., second ed .Cambridge Univ. Press, Cambridge, UK.

Rice, S.O., 1944. Mathematical analysis of random noise. Bell Syst. Tech. J. 23, 282 (Reprinted by N. Wax, Selected papers on Noise and Stochastic Process, Dover Publication, 1954. QA273W3).

Rowe, D.B., 2001. Bayesian source separation for reference function determination in fMRI. Magn. Reson. Med. 45 (5), 374–378.

Rowe, D.B., 2003. Multivariate Bayesian Statistics. Chapman and Hall/CRC Press, Boca Raton, FL, USA.

Rowe, D.B., 2005. Parameter estimation in the magnitude-only and complex-valued fMRI data models. NeuroImage (doi:10.1016/j.neuroimage.2004.12.048).

Rowe, D.B., Logan, B.R., 2004. A complex way to compute fMRI activation. NeuroImage 23 (3), 1078–1092.

Rowe, D.B., Logan, B.R., 2005. Complex fMRI analysis with unrestricted phase is equivalent to a magnitude-only model. NeuroImage 24 (2), 603–606.